



# Role of step stiffness and kinks in the relaxation of vicinal (001) with zigzag [110] steps



B. Mahjoub<sup>a</sup>, Ajmi BH. Hamouda<sup>a,b,\*</sup>, TL. Einstein<sup>b,c</sup>

<sup>a</sup> *Quantum Physics Laboratory, University of Monastir, Monastir 5019, Tunisia*

<sup>b</sup> *Department of Physics, University of Maryland, College Park, MD 20742-4111, USA*

<sup>c</sup> *CMTC, University of Maryland, College Park, MD 20742-4111, USA*

## A B S T R A C T

We present a kinetic Monte Carlo study of the relaxation dynamics and steady state configurations of  $\langle 110 \rangle$  steps on a vicinal (001) simple cubic surface. This system is interesting because  $\langle 110 \rangle$  (fully kinked) steps have different elementary excitation energetics and favor step diffusion more than  $\langle 100 \rangle$  (nominally straight) steps. In this study we show how this leads to different relaxation dynamics as well as to different steady state configurations, including that 2-bond breaking processes are rate determining for  $\langle 110 \rangle$  steps in contrast to 3-bond breaking processes for  $\langle 100 \rangle$ -steps found in previous work [Surface Sci. **602**, 3569 (2008)]. The analysis of the terrace-width distribution (TWD) shows a significant role of kink-generation-annihilation processes during the relaxation of steps: the kinetic of relaxation, toward the steady state, is much faster in the case of  $\langle 110 \rangle$ -zigzag steps, with a higher standard deviation of the TWD, in agreement with a decrease of step stiffness due to orientation. We conclude that smaller step stiffness leads inexorably to faster step dynamics towards the steady state. The step-edge anisotropy slows the relaxation of steps and increases the strength of step-step effective interactions.

## 1. Introduction

Zigzag  $\langle 110 \rangle$  steps on a vicinal (001) simple cubic lattice with only nearest-neighbor interactions allow step-edge fluctuations (with geometric constraints) which have no energy cost, a situation which does not hold for straight  $\langle 100 \rangle$  steps [1–3]. This suggests the possibility of different relaxation dynamics and steady state configurations for zigzag steps. A deeper understanding of steps is, of course, relevant to the study of surface nanostructures and is therefore technologically important. Indeed, the physical properties of epitaxial thin films can be manipulated by the understanding of the interfacial strain on the grown material. However, the strain can be controlled by adjusting the miscut angle of the vicinal substrate prior to growth. For example, anisotropic dielectric properties were observed and attributed to different tetragonalities induced by the vicinal substrate (LaAlO<sub>3</sub>) with miscut orientations along the  $\langle 100 \rangle$  and  $\langle 110 \rangle$  directions with different miscut angles [4]. Moreover, different nanostructuring behaviors were obtained depending on the step-orientation [5,6].

Metropolis Monte Carlo [7–11] was used long ago to study step-edge equilibrium properties as a function of orientation. Subsequent kinetic Monte Carlo (kMC) [12] studies of  $\langle 100 \rangle$  steps considered the

evolution to equilibrium. Here we apply kMC [13] to the study of  $\langle 110 \rangle$  steps on a vicinal (001) simple cubic surface in order to investigate the change in behavior due to distinctly different step-edge fluctuations.

This study is further motivated by investigations of flexible chains in a 2-D system [14] and interfacial configurations in a 2-D Ising ferromagnet on a square lattice [15], in which the primary observables of interest are interface energy and interface tension as functions of interface orientation. For a 2-D Ising ferromagnet, the surface tension depends on direction, being minimized along the  $\langle 110 \rangle$  direction and maximized along the  $\langle 100 \rangle$  direction. Returning our attention to surfaces, interface free energy per unit area, is used in the Wulff construction, yielding minimal free energy domain shapes at equilibrium [16,17].

The fluctuation behavior of steps underpins the self-assembly and control of nanostructures. The stiffness determines how a step responds to interactions with other steps, to atomistic mass-transport processes, and to external driving forces [18–20]. Atomic-scale simulations can address comprehensively this problem and provide a complete and fairly accurate database of step stiffness and its anisotropy, providing an alternative to experiment. A precise knowledge of step stiffness, including its anisotropy, is thus an essential ingredient for determining the dynamics of stepped surfaces using the continuum step model and/or simulations. In fact, the

\* Corresponding author.

E-mail address: [Ajmi.hamouda@fsm.rnu.tn](mailto:Ajmi.hamouda@fsm.rnu.tn) (A.B. Hamouda).

attachment-detachment mechanisms of atoms at step edges depend strongly on the kinetics at step edges, thus on the step stiffness. Therefore, the measurement of this latter is very important for describing step fluctuations, since it might contain valuable information about the dynamics of the surface and particularly some details concerning the main processes governing the motion of atoms and the fluctuation of steps [21].

The relationship between step orientation and step-edge stiffness has been the subject of extensive experimental and theoretical studies [22–26]. These works showed that steps which deviate from the close-packed direction have a smaller line tension and are less stiff, allowing more step wandering. Hence,  $\langle 110 \rangle$ -steps are significantly less stiff than  $\langle 100 \rangle$  steps.

In addition,  $\langle 110 \rangle$  steps have different elementary excitation energetics than  $\langle 100 \rangle$  steps. For  $\langle 110 \rangle$  steps,<sup>1</sup> an elementary excitation breaks 2 nearest-neighbor bonds and then reforms 2 nearest neighbor bonds, leaving the step length invariant. However, for  $\langle 100 \rangle$  steps an elementary excitation breaks 3 nearest neighbor bonds, and then reforms 1 nearest-neighbor bond, increasing the step length by 4 links. See Fig. 1 for images of an initial configuration of zigzag steps, as well as the same steps following an elementary excitation. To the extent that step energy depends only on the step length [14,27], elementary excitations of  $\langle 110 \rangle$  steps cost no energy, in contrast to elementary excitations of  $\langle 100 \rangle$  steps.

Moreover, the steps are taken to have entropic repulsions along the step edges, since steps cannot cross (although they can touch at corners or links). The step touching that is allowed in our model gives rise to an effective (finite-size correction) attractive interaction between steps, in comparison to the non-interacting (free fermion) model that we consider [27]. It should be noted that  $\langle 100 \rangle$  straight-steps were studied earlier by the present authors [12] and are used here only for comparison purposes. So only the results concerning  $\langle 110 \rangle$  zigzag-steps are novel.

The scheme of this paper is as follows: In Section 2 we describe the computational details of our kMC model for two orientations of steps along the  $\langle 100 \rangle$  and  $\langle 110 \rangle$  directions; then we present the theoretical model of the step stiffness adopted in this work in Section 3. Section 4 is devoted to an extensive study of the step dynamics by means of the TWD computation during step relaxation with a special focus on the steady state regime; along with a comparison between the two orientations. In Section 5, we check our previous results with step-stiffness measurements. A conclusion is given in Section 6.

## 2. Computational details

The 2-D solid-on-solid (SOS) model for  $\langle 110 \rangle$  steps assigns an integer height  $h(\vec{r})$  to each point  $\vec{r}$  on a square grid with zigzag edges of size  $L_x \times L_y$  embedded in a larger square grid, as depicted in Fig. 1. We use “Maryland notation” to assign Cartesian directions [12] in which the  $\hat{y}$  direction is along the mean step direction and  $\hat{x}$  is orthogonal to  $\hat{y}$ , pointing upstairs. We adopt periodic boundary conditions in the  $\hat{y}$  direction and screw-periodic boundary conditions in the  $\hat{x}$  direction. The fundamental length units are the lattice constant  $a \equiv 1$  and  $a_z = a\sqrt{2}$  (see Fig. 2).

The system Hamiltonian is written [12]:

$$H = \frac{E_a}{2} \sum_{\vec{r}, \vec{\delta}} |h(\vec{r}) - h(\vec{r} + \vec{\delta})|, \quad (1)$$

where  $\vec{\delta}$  runs over the four nearest neighbors of a site. Unless specified otherwise in the text, for both step configurations we used surfaces with the same step length along the  $\hat{y}$  direction and the same number of terraces in the  $\hat{x}$  direction (Fig. 3).

The system sizes are  $L_y = 5000$  and  $L_x = 80$ , expressed either in

<sup>1</sup> In preliminary work [12], the terrace width is measured normal to the  $\langle 100 \rangle$  direction on  $\langle 110 \rangle$  steps, instead of the  $\langle 110 \rangle$  direction. In fact, the global behavior of the TWD remains unchanged because, qualitatively, the latter is independent of the direction with respect to which it is computed, but quantitatively (specifically its characteristic variance) should be slightly changed.

terms of  $a$  for straight steps or  $a_z = a\sqrt{2}$  for zigzag steps; this means, we used 10 terraces of average width  $\langle w \rangle = 8a$  or  $\langle w \rangle = 8a_z$ . The other simulation parameters are:  $E_d = 1\text{eV}$ ,  $E_a = 0.35\text{eV}$ ,  $T = 580\text{K}$ , where  $E_d$  and  $E_a$  are the terrace diffusion and nearest-neighbor bonding energy barriers, respectively, for atom motion, and  $T$  the surface temperature.

These energetic barriers are typical values for silicon; however, we expect that this study should be applicable to a wide range of materials. For specific simulations, as in Figs. 5–7, we used:  $0.9\text{eV} \leq E_d \leq 1.1\text{eV}$ ,  $0.3\text{eV} \leq E_a \leq 0.42\text{eV}$  and  $520\text{K} \leq T \leq 580\text{K}$ . As depicted in Fig. 2-b, relevant lengths for zigzag steps are defined such that [28]:  $a_{||} = a_{\perp} = a/\sqrt{2}$  (note that for straight steps,  $a_{||} = a_{\perp} = a$ ).

The value of  $L_y$  is suitably large: it is chosen to be larger than the collision length  $y_{coll}$  [7] which is estimated in the next section. The choices of temperature and the range of energetic barriers follow similar kMC investigations of vicinal surfaces [12,29,30] to allow direct comparison with prior kMC results on straight steps. The temperatures used here are also the same as in other kMC simulations involving different shape dynamics; such as the shape relaxation of 2D islands [31] and 3D crystallites [32].

The surface is evolved to steady state using a rejection free kMC scheme [12], allowing step touching and but no vertical overhangs (i.e., two neighboring steps can touch along links at a given  $y$ -value but they cannot cross), leading to entropic repulsions between steps. Atoms with  $i = 4$  lateral nearest neighbor bonds are “frozen in” (not allowed to move). Furthermore, sublimation is forbidden. We have examined two cases: with symmetric and asymmetric step edge attachment (i.e., with an Ehrlich-Schwobel (ES) barrier hindering atoms from crossing steps downward). Atoms with  $i = 0, 1, 2, 3$  nearest neighbor bonds are chosen at random with a probability proportional to  $\exp[-(E_d + iE_a + E_{ES})/k_B T]$  and subsequently allowed to move with equal probability in any one of four nearest-neighbor directions. Since  $E_d/k_B T$  is the same for all moving atoms (adatoms),  $E_a/k_B T$  (and eventually the ES energy  $E_{ES}$ ) is what is expected to govern adatom motion and, therefore, step relaxation. Lattice configurations having double-valued  $x(y)$  (e.g., islands and multiple ledges as in Fig. 2-b) were discarded in our measurements.<sup>2</sup> Also, 100 MCS  $\rightarrow$  1 second was defined as the unit of time in the simulations [12].

## 3. Step stiffness model

Since we are trying to compare zigzag steps with straight steps (rather than do a comprehensive simulation study such as needed to determine relaxation exponents [28,33]),  $\langle w \rangle$  was chosen large enough to allow continuum modeling while also maintaining computational tractability. Given that  $L_y$  dependence of observables (once large enough) was not noted in earlier kMC work on straight steps [12],  $L_y = 5000a$  (or  $5000a_z$ ) was left fixed for both step configuration runs.

The lattice width  $L_y$  should be greater than the “collision length”,  $y_{coll}$ , the length in the  $\hat{y}$  direction for a step to wander a distance  $\langle w \rangle/2$  (in the  $\hat{x}$  direction). For straight steps we refer to an earlier terrace-step-kink (TSK)-based estimation [12] to show that  $L_y$  for our straight step runs is greater than the collision length, we found  $y_{coll}^{str} = 250a$  (for  $T = 580\text{K}$ ,  $E_a = 0.35\text{eV}$  and  $\langle w \rangle = 8a$ ). For zigzag steps, we estimate the collision  $y$  length to be about  $y_{coll}^{zig} = 36\sqrt{2}a = 36a_z$  for all temperatures and energies [7]; thus, it is significantly smaller than the lattice length  $L_y = 5000a_z$ . This calculation was based on the terrace definition and corresponding terrace width measurement scheme (see Fig. 2) due to Abraham et al. [27] and guided by an earlier study [7], in which the step-position correlation function (mean square displacement as a function of distance  $y$  along the step) is defined as:

<sup>2</sup> In fact, our simulation model does not reject such provisional (temporary) configurations, but they are neglected during our TWD measurements because their number is insignificant since an isolated atom configuration (without nearest neighbor bonds) does not represent a favorable (permanent) position for a moving atom.

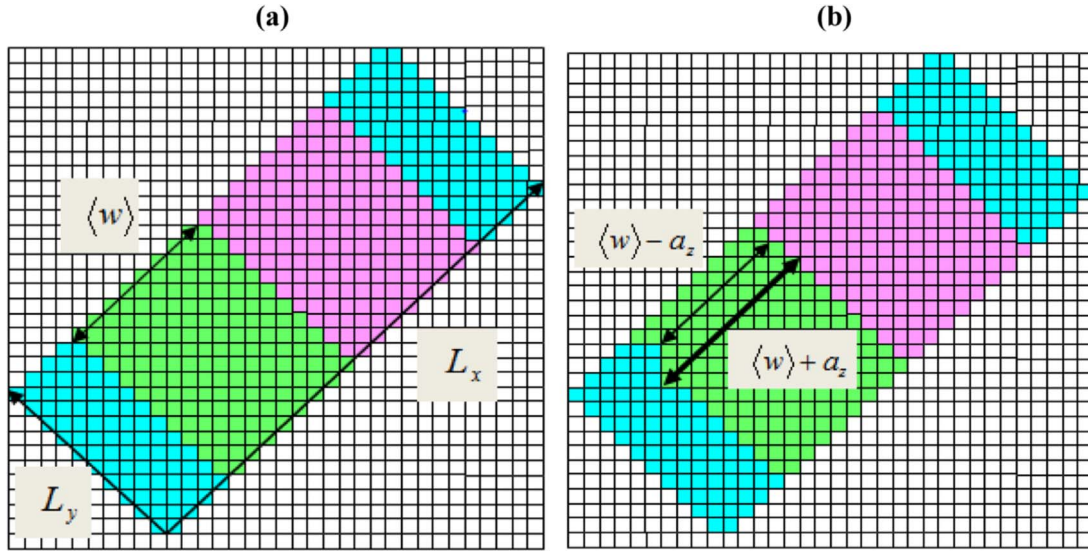


**Fig. 1.** (a) Initial, unexcited zigzag steps before any kMC evolution.  $L_y = 10a_z$  and  $L_x = 3\langle w \rangle = 24a_z$ ,  $L_y$  spans the length of a single step and  $L_x$  goes from the base of the bottom step to the top of the highest step. This figure displays 3 steps, with all terrace widths  $\langle w \rangle = 8a_z$ . In the  $\hat{y}$  direction there are periodic boundary conditions. Screw-periodic boundary conditions in the  $\hat{x}$  direction are applied when an atom diffuses out/off the top right or the lower left terrace (cyan). (b) The same set of zigzag steps as above, where one example of step excitation is now activated. This excitation annihilates 2 single terraces of length  $\langle w \rangle$  and generates 2 single terraces of length  $\langle w \rangle \pm a_z$  in the  $x$  direction.

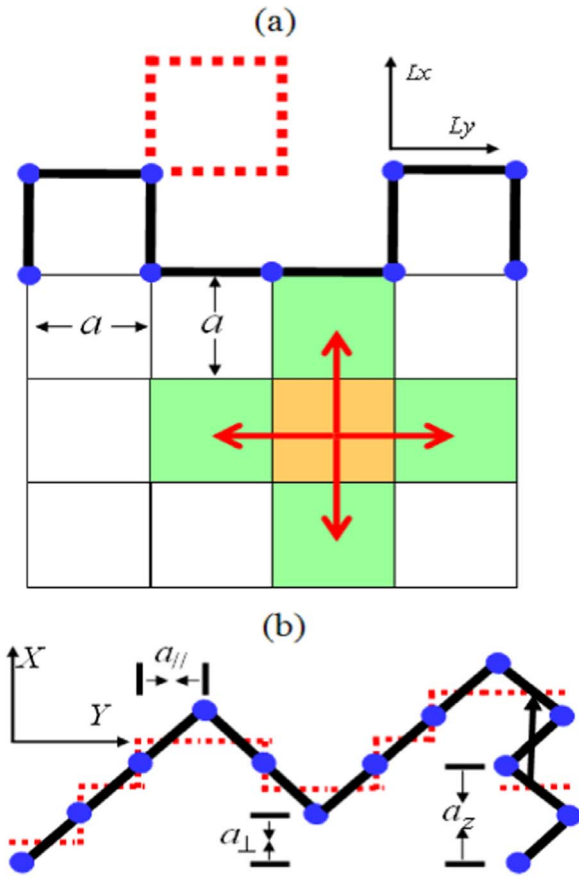


**Fig. 2.** (a) Depiction of straight steps. The thick line represents the step edge, with blue dots spaced distance  $a$  apart. The dashed red box is an island (isolated atom), which is a disallowed configuration because  $x(y)$  is double valued for those values of  $y$ . (b) Illustration of zigzag steps. Again, the thick line represents the step edge with the blue dots spaced distance  $a$  apart. Relevant lengths  $a_z$ ,  $a_{||}$  and  $a_{\perp}$  are also displayed. The dotted red line represents the mapping of zigzag step ledge to a straight ledge using the Abraham scheme [27] such that terrace width measurements can be determined straightforwardly. The dotted red lines, parallel to the  $\hat{y}$  direction connected by the vertical arrow at the far right of the figure is an example of a multiple ledge (forbidden since  $x(y)$  is double valued).

$$G_x(y) = \langle [x(y) - x(0)]^2 \rangle = \frac{k_B T}{\tilde{\beta} a_{||}} a_{||} y, \quad (2)$$

with  $x$  again the coordinate perpendicular to the mean orientation of the step profile and  $y$  the coordinate parallel to it. For a short distance  $y$ , we have diffusive step relaxation (random walk) and the correlation function behavior for  $G_x(y)$  is found to be linear with  $y$  and has the form [7]:

$$G_x(y) = \frac{b^2(T)}{a_{||}} y, \quad (3)$$

where  $b^2(T)$  is the mean square perpendicular deviation with each pace forward by  $a_{||}$  along the step (or the diffusivity). The behavior of Eq. (3) is verified in our simulations (Fig. 8-b); the step edge stiffness related to the diffusivity via:

$$\tilde{\beta} = \frac{k_B T}{b^2} a_{||} \quad (4)$$

The diffusivity is given as an expectation value weighted over all possible values of the kink size. Specifically for a kink of size  $n$  (or length  $na_{\perp}$ ), with energy  $E(n)$ :

$$\tilde{b}^2(T) = \frac{b^2(T)}{a_{\perp}^2} = \frac{2 \sum_{n=1}^{\infty} n^2 \exp\left(-\frac{E(n)}{k_B T}\right)}{1 + 2 \sum_{n=1}^{\infty} \exp\left(-\frac{E(n)}{k_B T}\right)} \quad (5)$$

where  $a_{\perp}$  is unit length perpendicular to the step. For straight steps, in the TSK approximation  $E(n) = |n|\epsilon$  ( $\epsilon = E_d/2$  and  $n=1, \dots, \infty$ ), this becomes [7,12]:

$$\tilde{b}_{st}^2(T) = \frac{2 \exp\left(\frac{\epsilon}{k_B T}\right)}{\left(\exp\left(\frac{\epsilon}{k_B T}\right) - 1\right)^2} = \frac{1}{2} \sinh^{-2}\left(\frac{\epsilon}{2k_B T}\right) \quad (6)$$

For zigzag steps, the preceding TSK analysis is inappropriate. Since for each pace forward  $a_{||}$  along the step (in  $\hat{y}$  direction), the step is displaced by a single unit  $a_{\perp}$  (in the absence of multiple ledges as illustrated in Fig. 2(b)), then the expectation value in this Modified Restricted Model becomes ( $n=1$ ):

$$\tilde{b}_{zig}^2(T) = \frac{2}{\exp\left(\frac{\epsilon}{k_B T}\right) + 2} \quad (7)$$

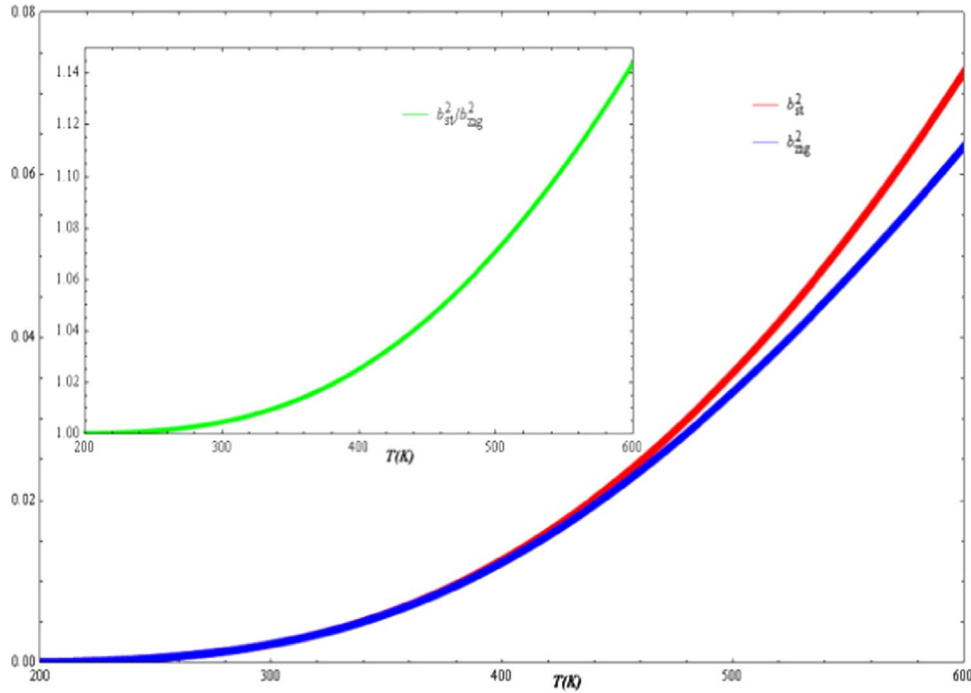


Fig. 3. Diffusivity vs. temperature (Eqs. (6) and (7)) for straight and zigzag steps. The inset shows their ratio, roughly equals 1 for 520K≤T≤580K).

For  $T \geq 500\text{K}$ ,  $\tilde{b}_{st}^2(T) \approx 2 \exp\left(\frac{-2e}{k_B T}\right)$  and  $\tilde{b}_{zig}^2(T) \approx 2 \exp\left(\frac{-e}{k_B T}\right)$ .

Therefore we obtain our Modified Restricted Model for the collision length, estimated by putting  $G_x(y) = \langle w \rangle^2/4$  into Eq. (3):

$$\chi_{coll} \equiv \frac{\langle w \rangle^2 a_{ll}}{4b^2(T)}. \quad (8)$$

By subsequently inserting values for  $\langle w \rangle^2, a_{ll}$  and  $b^2(T)$ , we can deduce the collision length for zigzag steps. Note, for no kinks of size zero (the 1 in denominator is absent), one obtains:  $b_{zig}^2(T) = a_{\perp}^2$ , which means that the diffusivity is the same for all energies and temperatures as predicted theoretically in Ref. [34] and confirmed in Ref. [35]. Since  $\langle w \rangle = 8a_z$  and  $a_{\perp} = a_{ll} = \frac{a}{\sqrt{2}}$ , one easily obtains the collision length estimate for zigzag steps cited earlier in the section.

Moreover,  $\frac{\tilde{b}_{st}^2(T)}{\tilde{b}_{zig}^2(T)} = \frac{1 + 2 \exp\left(\frac{-e}{k_B T}\right)}{\left(1 - \exp\left(\frac{-e}{k_B T}\right)\right)^2}$  roughly equals 1 for  $T < 400\text{K}$  and reaches 1.14 at  $T=600\text{K}$  (See Fig. 3) (between 1.08 and 1.12 for  $520\text{K} \leq T \leq 580\text{K}$ ); therefore, using Eq. (4), the stiffness ratio is approximately:

$$\frac{\tilde{\beta}_{zig}}{\tilde{\beta}_{st}} = \frac{(a/\sqrt{2}) \tilde{b}_{st}^2(T)}{a \tilde{b}_{zig}^2(T)} \approx \frac{1}{\sqrt{2}}.$$

## 4. TWD analysis

### 4.1. Dynamic results

In this section, we consider the relaxation to steady state for the zigzag steps, compare it with that of straight steps, and examine the implications of the time scales with which this relaxation occurs. The first item we consider is the evolution of the standard deviation of the terrace width distribution (TWD) to its steady state values.

Analytical and simulation results, studying the evolution of the variance of the TWD for different physically interesting and experimentally testable examples, have been achieved [10,12,33]. The steady-state solution of the probability density of the TWD is the generalized Wigner surmise describing the probability of finding neighboring steps

at a specified separation  $s=w/\langle w \rangle$ , states [10]:

$$P_{\rho}(s) = a_{\rho} s^{\rho} \exp(-b_{\rho} s^2), \quad (9)$$

where the constants  $a_{\rho}$  and  $b_{\rho}$  assure unit mean and normalization, can be expressed in terms of Gamma functions. In principle, the parameter  $\rho$  (typically called  $\beta$  in random matrix theory) describes the strength of the assumed inverse-square step-step interactions and so gives information about their sign and size.

To compare numerically simulated data with experimental data, one typically computes the standard deviation  $\sigma(t)$  of the distribution and then studies its time dependence. If the relaxation starts from an initial configuration of “perfect” straight steps, then  $\sigma(t)$  obeys [10]:

$$\sigma(t) = \sigma_{sat} \sqrt{1 - e^{-t/\tau}}, \quad (10)$$

where the saturation value  $\sigma_{sat}$  is the standard deviation for an infinite system at long time. When dealing with numerical data, we take the standard deviation to be normalized by the mean spacing, to mimic the formal analysis and deal with a dimensionless quantity. While  $\sigma_{sat}$  is related to the interaction strength,  $\tau$  provides crucial information for determining the main activated process of the dynamics [10,12].

Note that Eq. (10), established theoretically using a Fokker–Planck approach with a mean-field approximation [10], has been well verified for straight steps [12]. However, for zigzag steps, this expression no longer gives a good fit for our numerical results, specifically at early time, as shown in Fig. 5. Indeed, starting from a perfect zigzag steps (Fig. 4), a close analysis of step morphology in the early-stage regime, indicates the presence of two time constants. The first,  $\tau_1$ , is influential at short time and corresponds to a transient arrangement of steps during which the number of kinks per step decreases. The second,  $\tau_2$  ( $\tau_2 \gg \tau_1$ ), operates at longer time and governs the step relaxation to the steady state. Thus,  $\tau_2$  is the proper relaxation time constant. A slightly modified version of Eq. (10) containing three parameters (rather than two for straight steps) then suggests itself:

$$\sigma(t) = \sigma_{sat} \sqrt{1 - (e^{-t/\tau_1} + e^{-t/\tau_2})}, \quad (11)$$

where  $\sigma_{sat}$  is expected to depend on the step orientation.

Fig. 4 illustrates the morphology of  $\langle 110 \rangle$  steps, at temperature  $T=580\text{K}$ , early in the surface evolution ( $t < \tau_2$ ) before real relaxation becomes effective. We observe the formation of local facets along a step

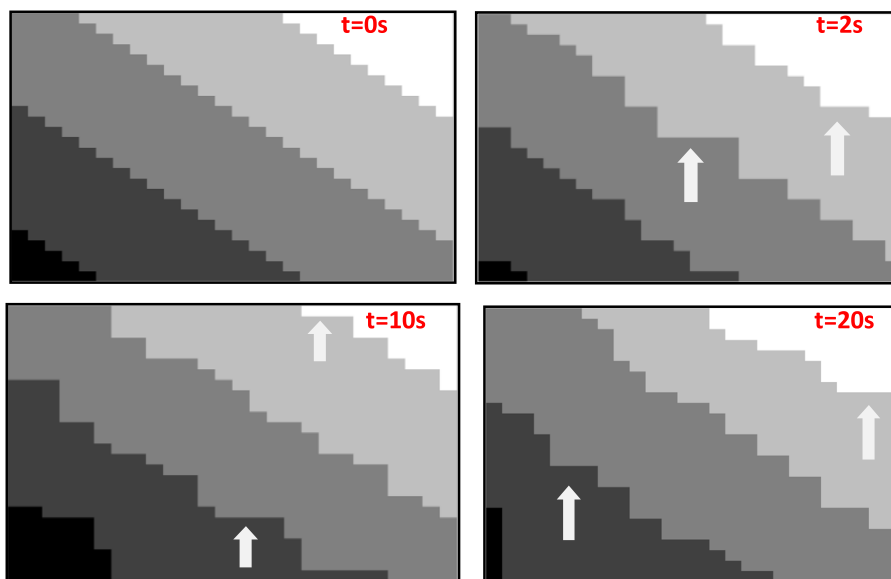


**Fig. 4.** Snapshots of the simulated morphology for the  $\langle 110 \rangle$  steps during early relaxation time  $t < \tau_2$  at temperature  $T=580$  K. We observe the formation of localized facets along step-edge (indicated by arrows). From left to right  $t=0, 2, 10$  and  $20$  s.

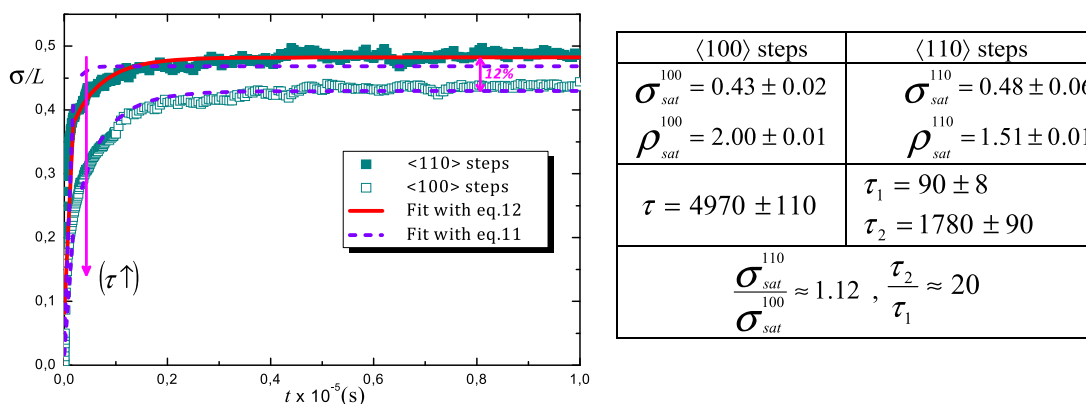


**Fig. 5.** Simulated standard deviation of the TWD vs. time (symbols) for zigzag and straight step systems, with examples of fits using Eq. (10) (dashed lines) and Eq. (11) (solid line), used to extract  $\tau$ . The standard deviation can be adjusted exactly with Eq. (10) for  $\langle 100 \rangle$  steps and Eq. (11) for  $\langle 110 \rangle$  steps. Simulation parameters are:  $E_d=1.0$  eV,  $E_a=0.35$  eV,  $T=580$  K,  $L=(w)$ . The system sizes are:  $L_y \times L_x=5000 \times 80$  expressed in  $(a_x \times a_x)$  and  $(a_x \times a_z)$  for straight and zigzag steps, respectively. Time  $t$  is essentially in seconds (see text).

edge (indicated by arrows), whose number increases with time. Our simulation results show that the ratio  $\tau_2/\tau_1$  is on the order of 20 (Fig. 5). Again,  $\tau_2$  is the physically significant rate describing the surface evolution to its steady state; it is the characteristic time that should be compared to the relaxation time constant  $\tau$  for the case of straight steps ( $\tau_2 \equiv \tau$ ). Since the characteristic time  $\tau_1$  depends on the initial configuration, it has no general meaning. Besides the difference in the magnitude of the relaxation time, we clearly note that as the zigzag system approaches steady state,  $\sigma$  reaches different saturation values. We measure a clear shift, on the order of 12%, in the standard deviation at infinite time between straight and zigzag steps.

The relaxation time  $\tau$ , i.e. the crossover time between growing and saturation of the fluctuations, is expected to depend typically on the longitudinal step length  $L_y$  in the context of surface growth [36,37]. In fact, it is possible that the relaxation parameters, especially the relaxation time, could exhibit finite-size effects. In order to avoid this issue, prior simulations were done by varying the system sizes, as it is shown in Ref. [12,29]; finally,  $L_y$  is chosen large enough for both step orientations. As for straight steps [12], we can use Arrhenius plots to determine which bond-breaking mechanism is the rate limiting process. The decay time is expected to exhibit Arrhenius behavior:  $\tau \propto \exp(E_b/k_B T)$ , where  $E_b$  is the activation barrier of the relaxation process. We investigate  $E_b$  closely in the two traces of Fig. 6 by ramping one simulation parameter while holding the others fixed. It is straightforward to deduce that the effective

energy barrier  $E_b$  is  $E_d+3E_a$  for straight steps (see Ref. [12] for more details) and  $E_d+2E_a$  for zigzag steps.

From Arrhenius analysis of the plots in Fig. 6, we immediately deduce  $\log(\tau) \propto (E_b/k_B T)$ , which implies that  $\tau \propto \exp[(E_d + 3E_a)/k_B T]$  for  $\langle 100 \rangle$  steps and  $\tau \propto \exp[(E_d + 2E_a)/k_B T]$  for  $\langle 110 \rangle$  steps, where the proportionality factor can be expressed in terms of  $\tau_0 = 10^{-13}$  s [10,12].

In summary, we reach the interesting conclusion that the equilibration of terraces on a vicinal (001) simple cubic crystal is closely linked to step orientation. Our analysis then shows that 2-bond breaking processes are rate-determining for  $\langle 110 \rangle$  steps, in contrast to 3-bond breaking processes for  $\langle 100 \rangle$ . Indeed, at equilibrium, the rate of the fluctuations is controlled primarily by the step stiffness, which is often used to describe the meandering of a step. The step stiffness describes the inertial resistance to meandering of the step and is closely related to the energy required to generate a kink in the step [18]. Moreover, the elementary process driving the step fluctuations is arguably linked to the transport of an atom from one kink to another, underpinning the diffusion of kinks along the step [36,37]. Thus, one would expect that the relaxation kinetics of steps towards equilibrium is also controlled (or at least affected) by the step stiffness. Since  $\beta$  depends on step orientation [34,38], it should contain further information about the relaxation kinetics of steps. To verify this reasoning, we compute the step stiffness in Section 5 for straight and zigzag steps.

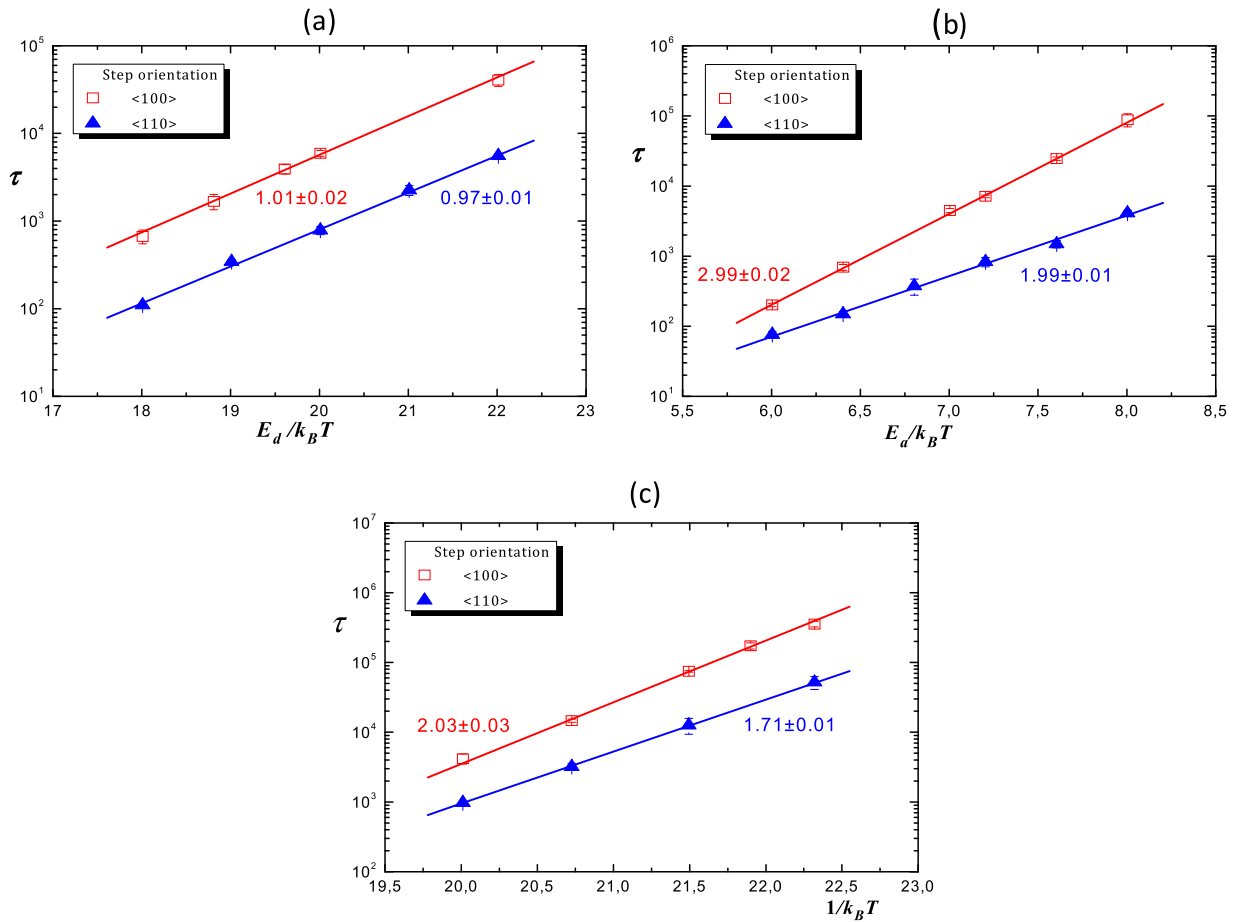


**Fig. 6.** Semi-log plots of the relaxation time  $\tau$  (in seconds) for the zigzag and straight step systems vs.  $E_d/k_B T$  at  $E_a=0.35$  eV (a) and vs.  $E_d/k_B T$  at  $E_a=1.0$  eV (b), where the temperature is maintained fixed for both systems at  $T=580$  K. (c) the relaxation time  $\tau$  versus  $1/k_B T$  for  $E_a=0.35$  eV and  $E_d=1.0$  eV, with temperature varied between 520 K and 580 K. The numbers inside the plots are slopes of the solid lines, best fits of the simulation data (symbols). From the slope of the fitted data, we determine the activation energy  $E_b$ , which is in excellent agreement with  $E_d+3E_a=2.05$  eV for  $\langle 100 \rangle$  steps; however,  $E_d+2E_a=1.7$  eV for  $\langle 110 \rangle$  steps. It is evident that 2-bond breaking processes are rate determining for zigzag steps, in contrast to 3-bond breaking processes for straight steps. The relaxation time is extracted from fitting the simulated variance in Fig. 5.

#### 4.2. Step-edge anisotropy effects

We finish this section with a brief analysis to see how the Ehrlich-Schwoebel barrier affects the variance of the TWD. Indeed, this mechanism, which offers a well-known way to break the upstairs-downstairs symmetry, can have important consequences in the evolution of surface morphology [30,39]. In our simulations, the resulting step-edge anisotropy is controlled through energy  $E_{ES}$ , ranging from 0 to 0.4 eV; we simulated four values 0.1, 0.2, 0.3, and 0.4 eV. The corresponding standard deviation is plotted (only for zigzag steps) in Fig. 7 versus  $E_{ES}$ , at  $T=580$  K,  $E_a=0.35$  eV and  $E_d=1$  eV. For all value of  $E_{ES}$ , good agreement is reached between the kMC data and the functional form proposed in Eq. (11). Similar good agreement (not displayed here) is obtained for straight steps with Eq. (10). The plots show a clear increase in the relaxation time  $\tau$  accompanied by a decrease of the saturation variance  $\sigma_{sat}$  of the TWD, when the anisotropy is increased at step-edges. This means that the increase of anisotropy slows down the step dynamics (i.e., longer relaxation time) and also increases the effective step-step interaction strength (i.e., bigger  $\rho$ , Table 1).

An interesting difference between the two step orientations is that for  $E_{ES} < \approx 0.1$  eV, step interactions are attractive for zigzag steps, whereas for straight steps they are always repulsive no matter the size of the ES barrier. Moreover  $(\frac{\tilde{\rho}_{st}}{\tilde{\rho}_{zig}})^{1/2} \approx 1.05$  for  $\rho > 2$ , which is roughly

equal  $\frac{\sigma_{zig}}{\sigma_{st}} = \frac{0.48}{0.43} = 1.11$ . This ratio can be also compared to  $(\frac{\tilde{A}_{zig}}{\tilde{A}_{st}})^{1/4} \approx 1.08$

for  $\rho \geq 3$ , in the regime where the Wigner distribution can be adequately approximated by the Gaussian distribution. Indeed, using the relation  $\sigma^4 \propto \frac{1}{\beta A}$  from the Gaussian approximation for the TWD [3], it is

straightforward to write:  $\frac{\sigma_{zig}}{\sigma_{st}} = \left( \frac{A_{st} \tilde{\rho}_{st}}{A_{zig} \tilde{\rho}_{zig}} \right)^{1/4}$ . Alternatively, from the predic-

tion  $(\frac{\tilde{\rho}_{st}}{\tilde{\rho}_{zig}}) \approx 2^{1/2}$ , we have,  $(\frac{\tilde{\rho}_{st}}{\tilde{\rho}_{zig}})^{1/4} = 2^{1/8} = 1.09$ . This means that the interaction anisotropy is almost included in the stiffness, i.e. in  $\tilde{A}$  rather than in  $A$ . Next, we focus on the influence of temperature on the stiffness.

#### 5. Step stiffness computation

In this section, we consider the case of no Ehrlich-Schwoebel barrier hindering atoms from crossing steps, with all other simulation parameters kept the same as in Section 2. Our goal is to compare the surface mass transport between straight and zigzag steps in order to confirm the difference in relaxation kinetics between  $\langle 100 \rangle$  and  $\langle 110 \rangle$  steps found previously in the TWD analysis.

We focus on steps moving under thermal excitation; this means that the surface steps are considered as entities which can move by mass transport between them. Step stiffness can be used as a gauge for step bending. For isolated steps, arguably the most important parameter is the step stiffness, which measures how easily a step fluctuates or wanders perpendicular to its mean orientation [38]. At finite temperature, steps on vicinal surfaces relax toward their equilibrium (steady) state. This relaxation is dictated by the surface energetics and the step stiffness, which controls the relative amplitude of fluctuations about the equilibrium shape.

The mass transfer between step edges is assumed to be governed by the thermal energy. Indeed, the simplest conditions under which step motion can be observed are equilibrium conditions in which the step position

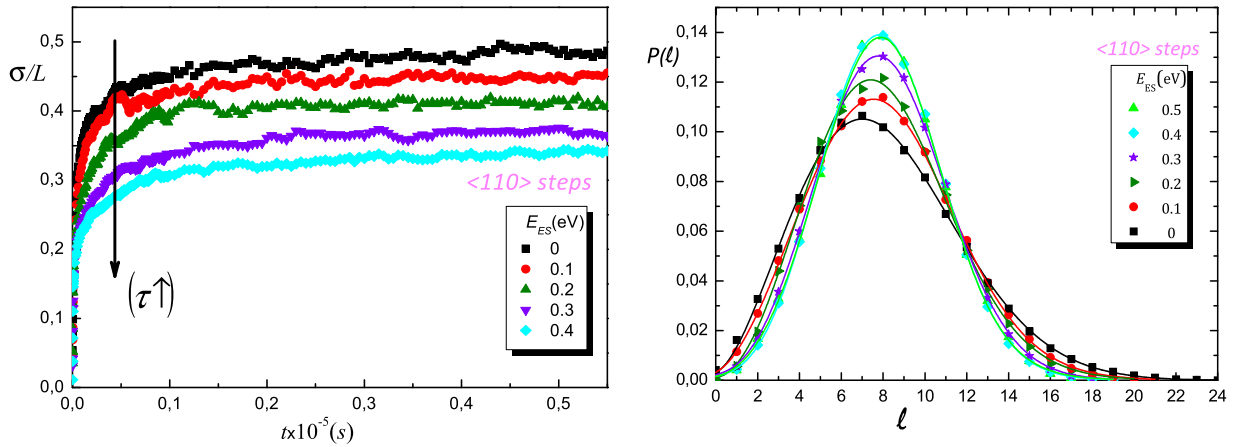


**Fig. 7.** Standard deviation (left) and the corresponding distribution at steady state (right) of the TWD for various Ehrlich–Schwoebel barrier ( $E_{ES}$ ) for zigzag steps at  $T=580$  K,  $E_a=0.35$  eV and  $E_d=1$  eV.  $L_x$  is the same as in Fig. 6, but here we used  $L_y=2000a_z$  rather than  $L_y=5000a_z$ . The distributions were fitted with the Wigner function (Eq. (9)). The fit parameter  $\rho$  is listed in Table 1.

**Table 1**

The fitting parameter  $\rho$  (Eq. (9)) of the TWD and the corresponding dimensionless interaction strength  $\tilde{A}$  vs. ES barrier for both step-orientations. From Refs. [4–7],  $\tilde{A} = \frac{A\tilde{\beta}}{(k_B T)^2} = \frac{\rho}{2} \left( \frac{\rho}{2} - 1 \right)$ , where  $A$  is the interaction strength and  $\tilde{\beta}$  the step-stiffness.

$E_{ES}$ (eV)	< 100 > steps		< 110 > steps	
	$\rho$	$\tilde{A}$	$\rho$	$\tilde{A}$
0	$2.00 \pm 0.01$	$0.00 \pm 0.00$	$1.51 \pm 0.01$	$-0.18 \pm 0.01$
0.1	$2.13 \pm 0.04$	$0.07 \pm 0.02$	$1.92 \pm 0.03$	$-0.03 \pm 0.02$
0.2	$2.43 \pm 0.06$	$0.26 \pm 0.04$	$2.25 \pm 0.05$	$0.14 \pm 0.04$
0.3	$3.01 \pm 0.08$	$0.76 \pm 0.08$	$2.80 \pm 0.07$	$0.56 \pm 0.08$
0.4	$3.49 \pm 0.10$	$1.30 \pm 0.12$	$3.18 \pm 0.09$	$0.93 \pm 0.08$
0.5( $\infty$ )	$3.52 \pm 0.10$	$1.34 \pm 0.13$	$3.21 \pm 0.10$	$0.97 \pm 0.10$

fluctuates due to thermal excitations. The variation of the step position  $x$  is accompanied by a variation in the total step length; then, to determine the step stiffness, it is convenient to use the spatial step-edge correlation function of the step profiles  $x(y)$ . The equilibrium thermal fluctuation of an isolated step allows the measurement of the step stiffness. This latter is measured from the fit of the mean-square displacement spatial function  $G_x(y)$  at small distances, which increases linearly with  $y$  [7].

From our kMC simulations at steady state, we have computed the step auto-correlation function,<sup>3</sup>  $G_x(y)$ , whose expression is given in Eq. (2). The data used for determining the step displacement  $x(y)$  are taken from the same surface profiles used for extracting the TWD. In Fig. 8a we plot the step-position correlation functions for <100>-straight and <110>-zigzag step at steady state for two temperatures  $T=580$  K and  $T=520$  K and with same lattice sizes used in Fig. 7. The correlation function evidently increases with temperature for both steps orientation. At fixed temperature, the plot for zigzag steps shows more oscillations than for straight steps, which means that zigzag steps exhibit more fluctuations, consistent with larger TWD seen in Fig. 7. Fig. 8b is the zoom of Fig. 8a for small distances  $|y|$  along the step, where the stiffness is extracted from the slope of each plot. Evidently, the inverse of the stiffness increases with increasing temperature, in qualitative agreement with the theoretical predictions [38].

<sup>3</sup> For both zigzag and straight steps,  $G_x(y)$  increases linearly at small distances along the step (we emphasize that within this distance, which sets the appropriate length scale for measuring the stiffness, step collisions are ignored), consistent with diffusive behavior in  $y$  (i.e. in the fictitious time associated with the mapping of steps to the world lines of 1D spinless fermions) [7]. The linear behavior is found over a  $y$  range much larger than the average step-step distance (approximately 46nm) while for larger  $y$  values the linear dependence ceases, in qualitative agreement with theory [7]. The slope is clearly greater for zigzag steps than straight steps, consistent with the Modified Restricted Model for zigzag steps and how it differs from the TSK theory model appropriate for straight steps [36,40].

The inverse step-stiffness measurements are accomplished over the temperature range  $520 \leq T \leq 580$  for <100> and <110> steps; simulation results are listed in Table 2. As can be observed, fully kinked steps have smaller stiffness  $\tilde{\beta}_{<110>}$  than straight steps  $\tilde{\beta}_{<100>}$ . This result has been verified experimentally and theoretically in many works [38,40,41]; moreover, the ratio of the stiffness is almost independent of  $T$  and roughly  $1/\sqrt{2}$  in agreement with the prediction in Section 2 based on the Ising model [40]. Indeed, the step-edge fluctuations are very sensitive to the step stiffness, which is often used to describe the step mobility, but also to the density of kinks (that provide a source or sink of diffusing atoms). Since the step stiffness describes the resistance to meandering of the step and is closely related to the energy required to generate a kink in the step, weaker step stiffness should yield faster step dynamics.

These static measurements of the stiffness are consistent with our previous conclusions obtained from the TWD analysis and allow a better understanding of the underlying mechanisms governing the mass transport during step fluctuation, to which a considerable amount of work has already been devoted [21,25,42,43].

## 6. Conclusions

This work is motivated by experimental [24,44] and theoretical papers [38,45,46] showing that the step stiffness  $\tilde{\beta}$ , which governs step fluctuations, depends on both temperature and step orientation. To determine and clarify the dominant mechanism governing the relaxation of zigzag steps to steady state, we have performed kMC simulations of a solid-on-solid model which incorporates only nearest-neighbor interactions, previously employed to study the fluctuations of straight steps at equilibrium [12,30] and coarsening during unstable epitaxial growth [29,39]. Good agreement with recent theoretical and experimental results is found. Here, we have studied the change in the dynamics and steady-state properties of vicinal (001) simple cubic surfaces for which steps have zigzag orientation along <110> direction, in contrast to straight steps in the <100> direction. The relaxation kinetics and step-step interactions are analyzed through the TWD and within a mean-field approach [10]. We showed that fluctuations of zigzag steps are much more pronounced than those of fluctuate much easier than straight steps and are activated by 2-bond (rather than 3-bond for straight steps) breaking processes as the rate determining. Our results prove that relatively small step stiffness, as in the case of zigzag steps, imperatively leads to faster the step dynamics; where kink-generation processes seem to play a significant role in the step equilibration. Step anisotropy is also found to slow the step dynamics and also to increase the effective step-step interaction strength.

The long-time saturation of the variance of the TWD ( $t > \tau$ ) indicates that the system has reached steady state, characterized by specific standard deviation and relaxation time constants. Both of them are affected,

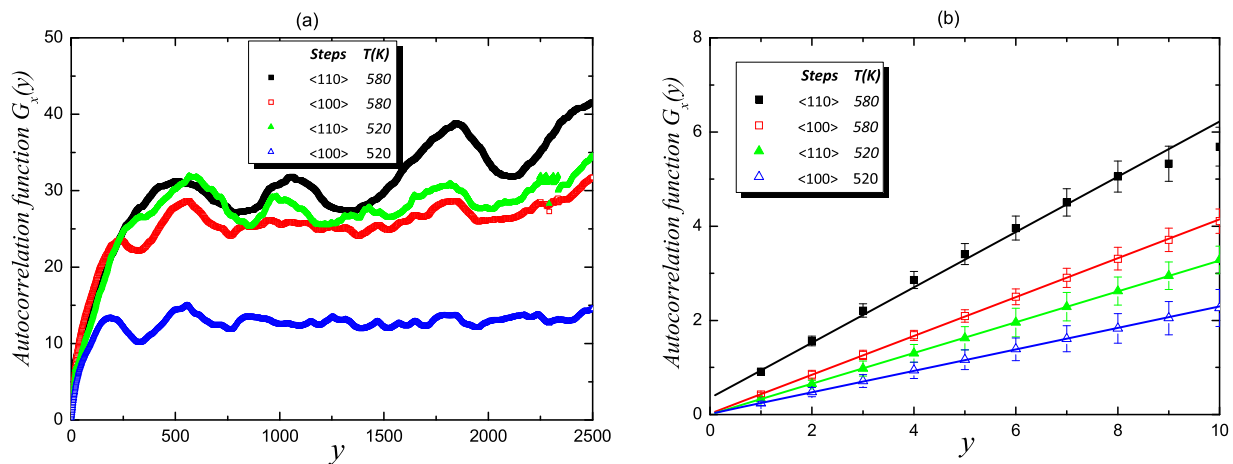


**Fig. 8.** (a) Step-position autocorrelation function  $G_x(y)$  vs. the coordinate  $y$  running parallel to step edges. Comparison between <110>-zigzag and <100>-straight step systems at steady state averaged over 20 steps, where  $E_{ES}=0$  eV and for two temperatures:  $T=580$  K and  $T=520$  K. (b) Zoom at small  $y$ , where the straight lines are linear fits of simulation data (symbols), with a slope of  $k_B T/\tilde{\beta}$ .

**Table 2**

Inverse step-stiffness ( $\pm 0.005$ ) for zigzag and straight steps at four temperatures. The stiffness ratio is almost independent of  $T$  and very close to  $1/\sqrt{2}$ .

$T$ (K)	$(k_B T/a)/\tilde{\beta}_{<100>}$	$(k_B T/a)/\tilde{\beta}_{<110>}$	$\tilde{\beta}_{<110>}/\tilde{\beta}_{<100>}$
520	0.224	0.328	0.683
540	0.276	0.397	0.695
560	0.326	0.466	0.699
580	0.409	0.589	0.694

eventually, by the presence of step-edge anisotropy and depend on the orientation of steps. They also prove to be a direct manifestation of step-stiffness properties and its precise dependence on energetic barriers. Indeed, the analysis of the stiffness for both step orientations confirms that zigzag steps have smaller stiffness than straight steps; in turn, this explains why the dynamics of steps is faster in the former case. Then, the stiffness behavior, which is also step-orientation dependent, provides more information about the step relaxation, in accordance with previous TWD results.

Our study presents comprehensive information for the microscopic mechanism driving the surface dynamics. Indeed, the step kinetics is governed essentially by the *generation-annihilation* of kinks, the steady state by the density and the distribution of kinks. There is some evidence that the density of kinks might affect the adatom mobility on the surface, consequently affecting the step-meandering instability during epitaxial growth. For more thorough understanding of the step relaxation and the significant role of kinks generation, this work will be extended by adding next-nearest-neighbor interactions, whose effect on the step-stiffness and step-meandering has been revealed recently [45] during growth of vicinal surfaces (far from equilibrium).

## Acknowledgments

The authors wish to acknowledge B. Oujia for his support in Monastir. Research at the University of Maryland was funded in part by NSF-CHE Grant no. 13–05892.

## References

- [1] S. Kodambaka, S.V. Khare, V. Petrova, D.D. Johnson, I. Petrov, J.E. Greene, *Phys. Rev. B* 67 (2003) 035409.
- [2] S. Kodambaka, V. Petrova, S.V. Khare, D.D. Johnson, I. Petrov, J.E. Greene, *Phys. Rev. Lett.* 88 (2002) 14.
- [3] M. Giesen, C. Steimer, H. Ibach, *Surf. Sci.* 471 (2001) 80.
- [4] G. Yao, Y. Ji, W. Liang, M. Gao, S. Zheng, Y. Wang, H. Li, Z. Wang, C. Chen, Y. Lin, *Nanoscale* 9 (2017) 3068.
- [5] N. Neel, T. Maroutian, L. Douillard, H.-J. Ernst, *J. Phys. Condens. Matter.* 15 (2003) S3227.
- [6] Chuan-Fu Lin, Ajmi B.H. Hammouda, Hung-Chih Kan, N.C. Bartelt, R.J. Phaneuf, *Phys. Rev. B* 85 (2012) 085421.
- [7] N.C. Bartelt, T.L. Einstein, E.D. Williams, *Surf. Sci.* 276 (1992) 308.
- [8] N.C. Bartelt, T.L. Einstein, E.D. Williams, *Surf. Sci. Lett.* 240 (1990) L591.
- [9] N.C. Bartelt, T.L. Einstein, E.D. Williams, *Surf. Sci.* 312 (1994) 411.
- [10] A. Pimpinelli, H. Gebremariam, T.L. Einstein, *Phys. Rev. Lett.* 95 (2005) 246101.
- [11] J.A. Yancey, H.L. Richards, T.L. Einstein, *Surf. Sci.* 598 (2005) 78.
- [12] A.B.H. Hamouda, A. Pimpinelli, T.L. Einstein, *Surf. Sci.* 602 (2008) 3569 (*J. Phys. Condens. Matter* 20 (2009) 355001).
- [13] M. Biehl, A. Voigt (Ed.) *International Series of Numerical Mathematics: Multiscale Modeling in Epitaxial Growth* 149, Birkhauser, Switzerland, 2005, pp. 3–18.
- [14] P.G. DeGennes, *J. Chem. Phys.* 48 (1968) 2257.
- [15] D.B. Abraham, P. Reed, *J. Phys. A: Math. Gen.* 10 (1977) L121.
- [16] D.B. Abraham, *J. Stat. Phys.* 34 (1984) 793 (*Phys. Rev. Lett.* 5 (1983) 1279).
- [17] S.V. Khare, S. Kodambaka, D.D. Johnson, I. Petrov, J.E. Greene, *Surf. Sci.* 522 (2003) 75.
- [18] H.J.W. Zandvliet, R. Van Moere, Bene Poelsema, *Phys. Rev. B* 68 (2003) 073404.
- [19] H.J.W. Zandvliet, O. Gurlu, R. van Gastel, B. Poelsema, *Phys. Rev. B* 69 (2004) 125311.
- [20] H.J.W. Zandvliet, Frank R. van Dijk, Bene Poelsema, *Phys. Rev. B* 72 (2005) 113412.
- [21] A. Karim, M. Rusanen, Ismo T. Koponen, T. Ala-Nissila, T.S. Rahman, *Surf. Sci.* 554 (2004) L113–L119.
- [22] L. Persichetti, A. Sgarlata, M. Fanfoni, M. Bernardi, A. Balzarotti, *Phys. Rev. B* 80 (2009) 075315.
- [23] F. Szalma, D.B. Dougherty, M. Degawa, E.D. Williams, M.I. Haftef, T.L. Einstein, *Phys. Rev. B* 73 (2006) 115413.
- [24] M. Ondrejcek, M. Rajappan, W. Swiech, C.P. Flynn, *J. Appl. Phys.* 100 (2006) 083523.
- [25] M. Ondrejcek, M. Rajappan, W. Swiech, C.P. Flynn, *Phys. Rev. B* 73 (2006) 035418.
- [26] T.L. Einstein, *Appl. Phys. A* 87 (2007) 375.
- [27] D.B. Abraham, F.H.L. Eßler, F.T. Latremolière, *Nucl. Phys. B* 556 (1999) 411.
- [28] (a) Y.-L. Chou, M. Pleimling, R.K.P. Zia, *Phys. Rev. E* 80 (2009) 061602; (b) Y.-L. Chou, M. Pleimling, *J. Stat. Mech. : Theor. Exp.* (2010) P08007.
- [29] A. Hamouda, (Ph.D. thesis), Université Blaise Pascal, Clermont 2 (France), Doctoral School of Fundamental Science, No. 531, 2007.
- [30] Ajmi B.H. Hamouda, A. Pimpinelli, T.L. Einstein, *Europhys. Lett.* 88 (2009) 26005.
- [31] P. Jensen, N. Combe, H. Larralde, J.L. Barrat, C. Misbah, A. Pimpinelli, *Eur. Phys. J. B* 11 (1999) 497.
- [32] N. Combe, P. Jensen, A. Pimpinelli, *Phys. Rev. Lett.* 85 (2000) 110.
- [33] S. Bustingorry, P.M. Centres, *Phys. Rev. E* 84 (2011) 011613.
- [34] T.J. Stasevich, T.L. Einstein, R. Zia, M. Giesen, H. Ibach, F. Szalma, *Phys. Rev. B* 70 (2004) 245404.
- [35] M. Hawkins, A.B. Hamouda, T.L. Einstein, unpublished.
- [36] G.S. Verhoeven, J.W.M. Frenken, *Surf. Sci.* 601 (2007) 13.
- [37] A.-L. Barabási, H.E. Stanley, *Fractal concepts in surface growth*, Cambridge, 1995.
- [38] (a) T.J. Stasevich, T.L. Einstein, *SIAM: Multiscale Model. Simul.* 6 (2007) 90; (b) T.J. Stasevich, H. Gebremariam, T.L. Einstein, M. Giesen, C. Steimer, H. Ibach, *Phys. Rev. B* 71 (2005) 245414.
- [39] A. Videcoq, A. Pimpinelli, M. Vladimirova, *Appl. Surf. Sci.* 177 (2001) 213.
- [40] S. Dieluweit, H. Ibach, M. Giesen, T.L. Einstein, *Phys. Rev. B* 67 (2003) 121410.
- [41] S. Kodambaka, S.V. Khare, V. Petrova, A. Vailionis, I. Petrov, J.E. Greene, *Surf. Sci.* 513 (2002) 468.
- [42] M. Ondrejcek, W. Swiech, C.S. Durfee, C.P. Flynn, *Surf. Sci.* 54 (2003) 131.
- [43] M. Ondrejcek, W. Swiech, M. Rajappan, C.P. Flynn, *Phys. Rev. B* 72 (2005) 085422.
- [44] M. Al-Shakran, L.A. Kibler, T. Jacob, H. Ibach, G.L. Beltramo, M. Giesen, *Surf. Sci.* 651 (2016) 84.
- [45] S. Blel, A.B.H. Hammouda, B. Mahjoub, T.L. Einstein, *Phys. Rev. B* 95 (2017) 085404.
- [46] H. Ibach, M. Giesen, M. Al-Shakran, L.A. Kibler, T. Jacob, *Surf. Sci.* 659 (2017) 52.